Acoustic resonances in straight micro channels: Beyond the 1D-approximation

S. M. Hagsäter,[a] **A. Lenshof,**[b] **P. Skafte-Pedersen,**[a] **J. P. Kutter,**[a] **T. Laurell**[b] **and H. Bruus**[a]

Acoustic actuation can be used to perform several tasks in microfluidic systems. In this paper, we investigate an acoustic separator through micro-PIV analysis in stop-flow mode and numerical simulations, and a good agreement between the two is found. Moreover, we demonstrate that it is not sufficient only to characterize devices in flow-through mode, since in these systems much different resonant patterns can result in similarly looking band formations. Furthermore, we conclude that extended 1D approximations of the acoustic radiation force are inadvisable, and instead, a 2D model is preferred. The results presented here provide valuable insight into the nature and functionality of acoustic microdevices, and should be useful in the interpretation and understanding of the same.

I. Introduction

Acoustic actuation poses an attractive option for the performance of various relevant microfluidic tasks. Successful demonstrations of acoustic forces used for enrichment,[1,2] mixing,[3,4] cell handling,[5,6] medium exchange,[7] separation,[8–11] sorting[12] and others, have been provided.

However, the evaluation of these devices is mostly limited to quantifying and commenting on the net effect of the acoustic actuation in these systems as a whole, rather than investigating more locally how the desired effects are actually achieved. Moreover, numerical modeling of acoustic formation in the microfluidic designs has not been successfully reported, and, instead, the description of a sphere in a 1D standing wave[13–15] is typically supplied and described as extending uniformly for the whole length of a channel of constant width.[1,2,5,8–10]

In this work, we apply a recently reported method of investigation[16] for the examination of a previously well documented microchip based acoustic separator device.[8] We chose to work with this device as it has a non-complex design, which makes it attractive for both the experimental micro-PIV investigation and the numerical simulations. The device operates in continuous mode and has its function in that it can separate suspended particles from their medium. Moreover, the acoustic separator has seen a large number of successors,[7,9,12,17] intended for various microfluidic scenarios and functionalities, which makes it a suitable representative for a whole range of devices actuated and fabricated in a similar manner.[18] The results presented herein are foremost representative for these devices, but anticipate that similar behavior is to be expected and that the same conclusions are valid for other actuation variants and chip designs as well.

The current investigation has shown that the acoustic resonances are indeed of more complex nature than what is described by an extended 1D approximation. The experimental results were also found to agree with numerical 2D simulations. A discussion on this acoustic separator, and similar devices, is provided.

II. Materials and methods

The investigated acoustic separator was defined in a silicon substrate by the use of UV-lithography and chemical wet etching. After etching, the channel was sealed by a glass lid through anodic bonding, and silicone tubings were glued to the backside of the chip, for easy attachment of fluidic connections. A more detailed description of the fabrication process can be found in Nilsson *et al.*[8] A sketch of the microchannel and the surrounding silicon substrate is seen in Fig. 1.

The device was actuated by a piezo ceramic (Pz26, Ferroperm Piezoceramics, Kvistgard, Denmark), pressed to the backside of the chip and acoustically coupled *via* an ultrasonic gel (Aquasonic Clear, Parker Laboratories Inc., Fairfield, NJ) in between for good acoustic energy transmission. The transducer was biased by a signal generator (33250A, Agilent Technologies Inc., Santa Clara, CA), the effective power measured by a digital power meter (Model 5000-EX, Bird Electronic Corp., Cleveland, Ohio) and the amplitude monitored by an oscilloscope (TDS 210, Tektronix Inc., Beaverton, OR). More information on the experimental details, including piezo-actuation, can also be found in ref. 8.

A progressive scan interline CCD camera (Hisense MkII, Dantec Dynamics, Skovlunde, Denmark), mounted with a 0.63× tv-adapter onto a research microscope (DMLB, Leica Microsystems, Wetzlar, Germany), was used to record multiple sets of image pairs, used for the micro-PIV analysis. For the measurements presented in this paper, a relatively low magnification microscope objective (5×) was chosen, to allow a fairly large part of the microfludic channel to be recorded in each position. A pulsed blue LED (XLamp XR-E, Cree,

[a]Department of Micro- and Nanotechnology, Technical University of Denmark, DTU Nanotech Building 345 east, DK-2800, Kongens Lyngby, Denmark
[b]Department of Electrical Measurements, Lund University, Box 118, 221 00, Lund, Sweden
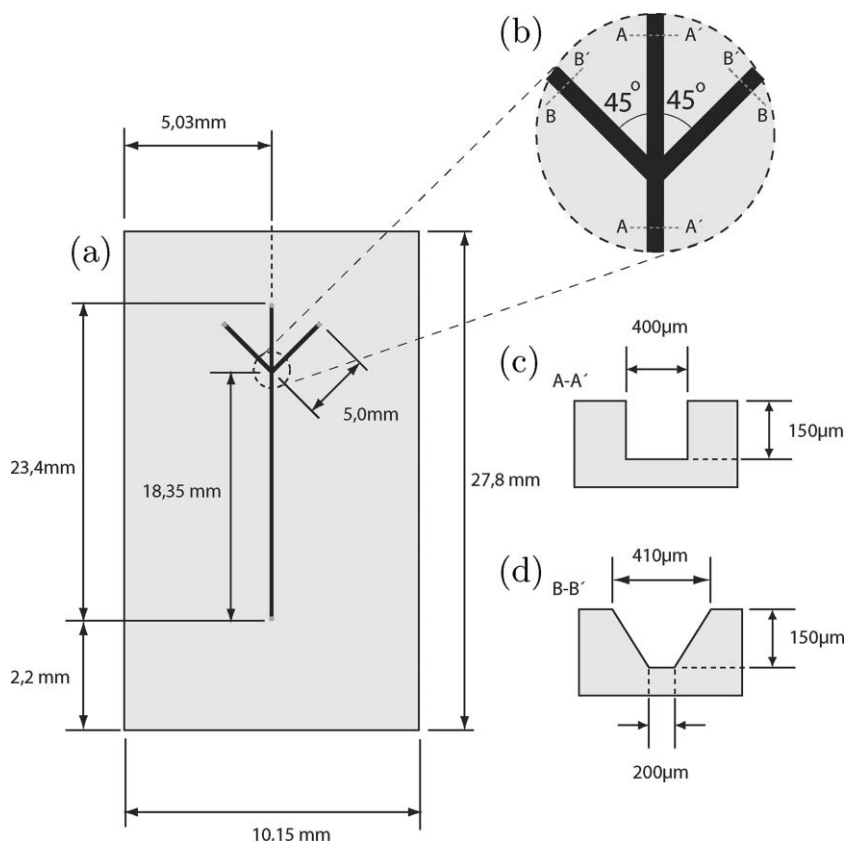
Fig. 1 Sketch with dimensions of the separation chip used in the experiments. (a) Top view of the micro-channel and the surrounding silicon substrate. (b) Close up in junction region. (c) Cross-sectional view of the main channel. (d) Cross-sectional view of the side channels.

Durham, NC), mounted in a front-lit configuration was used to illuminate the sample.[19]

For the separation efficiency measurements, the flow rate was controlled by a syringe pump (WPI SP210iwz, World Precision Instruments, Sarasota, FL), and injection valves (Rheodyne 7000, Cotati, CA) with a fixed loop volume were used to take samples. On the other hand, during the micro-PIV measurements, the same injection valves were used to stop the flow so that only particle motions created by acoustic effects were measured. As the acoustic radiation force scales with the volume of the particle, whereas the acoustic streaming is a motion of the fluid medium, the two respective forces can be distinguished from each other by applying tracer particles of different sizes. That is, the small particles will most likely mainly be affected by the motion of the fluid medium, whilst the primary motion of the larger particles will be from the radiation force. In this study two types of particles were used: 5 μm polyamide micro-beads (Danish Phantom design) and 1 μm fluorescent polystyrene micro-beads (Duke Scientific). The larger particles were also used in the separation efficiency measurements, where the number of particles passing through the middle and the side outlets, respectively, was counted using a Coulter counter (Multisizer 3, Beckman Coulter Inc., Fullerton, CA).

A detailed description of the special adaptations and considerations required when applying micro-PIV for the investigation of acoustic forces in microfluidic systems can be found in ref. 16. In the present work, unless stated otherwise, the same measurement scheme has been applied. Additionally, the 2D chip model, and

2D chamber model simulations, using COMSOL Multiphysics finite element software, have also been performed analogously to Hagsäter et al.[16]

III. Results and discussion

A. 1D approximation and 2D simulations

The most dominant acoustic effect for larger particles positioned inside an acoustic standing wave field is the acoustic radiation force.[13–15] For a one-dimensional standing planar acoustic wave, the force $\boldsymbol{F}_r$ on a sphere at the distance x from a pressure node can be described as,[14]

$$\boldsymbol{F}_r = -\left(\frac{\pi p_0^2 V_p \beta_m}{2\lambda}\right)\phi(\beta,\rho)\sin(4\pi x) \tag{1}$$

$$\phi(\beta,\rho) = \frac{5\rho_p - 2\rho_m}{2\rho_p + \rho_m} - \frac{\beta_p}{\beta_m} \tag{2}$$

where λ is the ultrasonic wavelength, p_0 is the pressure amplitude and V_p the volume of the sphere. The factor ϕ defines in which direction the particles will move, either towards or away from the pressure nodes, depending on the relation between the densities and compressibilities of the particle (ρ_p, β_p) and the medium (ρ_m, β_m).

This formula for a 1D wave is often used in the literature to describe the effect of the acoustic radiation force in microfluidic

channels.[1,2,5,7,8,11,12,17,22–25] Typically, the focusing effect is described as a confined extension of the 1D case along the length of the channel of frequency matching width. Acoustic effects are often not ascribed to the parts of the system where there is no frequency matching. The acoustic separator examined in this work described by the extended 1D model, with a channel width of 400 μm and a sound velocity in water of 1483 m s⁻¹ (20 °C), yields $\lambda = 800$ μm equivalent to an ideal frequency $f \sim 1.85$ MHz for half a wavelength over the width of the channel. Due to various loss mechanisms, frequency-broadening of the acoustic resonance will occur, but the model only suggests resonant solutions with half a wavelength separation in between.

An improved description of an acoustically actuated microfluidic system can be obtained by finding eigenmode solutions p_n to the Helmholtz eigenvalue equation $\nabla^2 p_n = -(\omega_n^2 / c_i^2) p_n$, where ω_n are the resonance angular frequencies, n is the mode number, and the index i of the sound velocities c_i is referring to the three material domains of silicon, water and glass in the chip.[16] This model of the system including the silicon substrate, water-filled microchannels and glass lid, we denote the 3D model. In the case where the height of the system is less than half of a wavelength, the description can be approximated by a simpler (not least in respect to the requisite of computational power) 2D approach, where the eigenvalue problem is solved only in the center plane of the microchannels and the surrounding silicon substrate. This second model we denote the 2D chip model. A further simplification is obtained by utilizing the large difference in acoustic impedance between water and silicon: the 2D Helmholtz eigenvalue equation is solved only for the fluidic part of the system, while the surrounding chip substrate appears only as a hard wall boundary condition on the walls of the microchannels. This third model we denote the 2D chamber model, and it is valuable, as it gives a more principal representation of the acoustic resonances that can be difficult to detect in the more complete 2D chip model. A justification for the two 2D models, based on the flatness of the system, as well as a more detailed description of how the numerical simulations should be interpreted in relation to experimental results is given in Hagsäter et al.[16]

If the Helmholtz eigenvalue equation is solved for the idealized 2D chamber model of the acoustic separator, the result is much different to that suggested by an extended 1D model. Instead of a single solution for one specific frequency, the 2D chamber model suggests several solutions within a rather wide frequency span. More specifically, instead of a uniform pressure amplitude along the length of the channel, the solutions display an increasing number of "pinching regions" along the channel (see Fig. 2). Starting at 1.85 MHz, where we have one full ($n = 1$) pinching region, solutions were identified for all integer values n, up to $n = 32$ for 2.25 MHz. The frequency shift between the solutions were in the range of 1.5–15 kHz, with a tendency of larger separations for higher frequencies. The calculated eigenfrequencies agree with the observed ones within one percent.

These solutions can be understood by considering that the acoustic eigenmodes in the channel system are dominated by, primarily, a transverse wavelength λ_t and a longitudinal wavelength λ_l contributing to the forming standing wave pattern. As the Helmholtz eigenvalue equation is modeled with a hard wall boundary condition, the resonant wavelengths will be
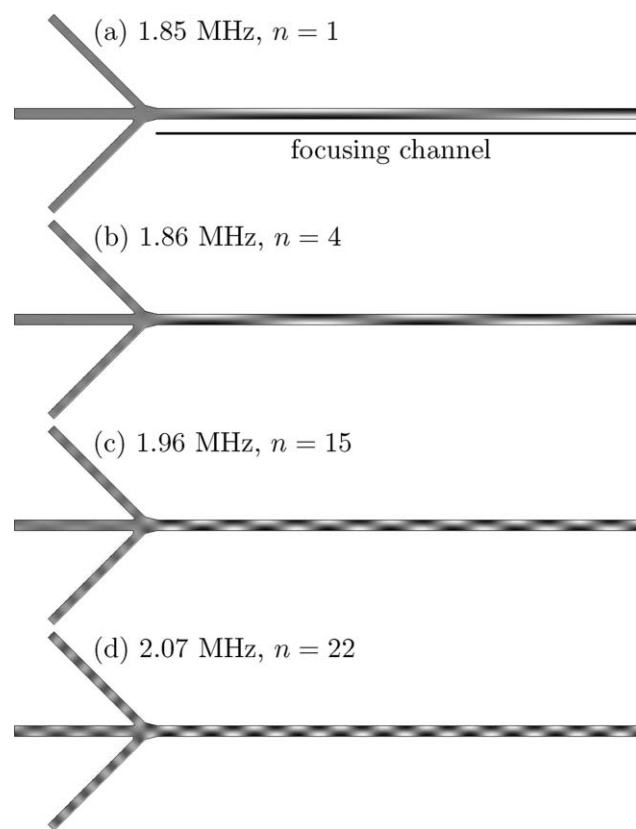
Fig. 2 Gray-scale plots of the pressure eigenmodes p_n for the chamber model at (a) 1.85 MHz, (b) 1.86 MHz, (c) 1.96 MHz and (d) 2.07 MHz. The integer value n is the number of pinching regions in the focusing channel.

fractions of the channel dimensions. The resonance frequencies f can be estimated by

$$f = c_w \sqrt{\lambda_t^{-2} + \lambda_l^{-2}} \quad (3)$$

where c_w is the sound velocity in water. We consider solutions for which there is half a standing wave over the width of the channel, thus $\lambda_t = 2w$ with $w = 400$ μm Similarly, we have $\lambda_l = 2L/n$, where $L = 18.3$ mm is the length of the focusing channel. Since $w \ll L$, f will be dominated by λ_t, and hence, a very small shift in frequency will result in a change of the number of pinching regions n. From this relation we can also conclude that if a microdevice is operated at a fixed frequency, even a small change in the temperature dependent sound velocity will cause a change in the number of pinching regions.

B. Device operated in flow-through mode

As a first investigation of the device, the chip was screened in flow-through mode, with continuous piezo actuation. The frequency of the AC voltage generator was scanned in the interval between 1.8 MHz and 2.2 MHz, while the separation effect was monitored. In the whole of this frequency span, a focusing effect of varying intensity was observed. In Fig. 3 stitched image frames recorded at three local maxima at a flow rate of 0.1 mL min⁻¹ are shown. Of these three, the strongest focusing effect was seen at 1.86 MHz, even though the transmitted power was set to a lower value for this frequency
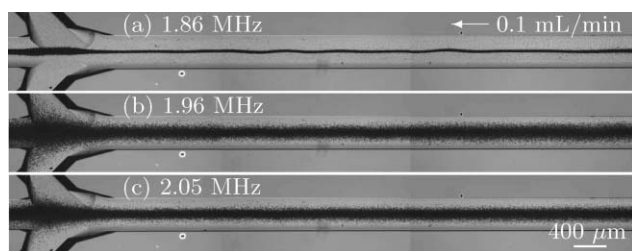
Fig. 3 The final 6 mm of the focusing channel leading up to the separation area of the device operating at frequencies of (a) 1.86 MHz, (b) 1.96 MHz and (c) 2.05 MHz. For comparison the same flow rate 0.1 mL min⁻¹ was used in all panels (a)–(c). The transmitted power was set to 0.5 W in (b) and (c), and to 0.2 W in (a), where a much stronger focusing effect was found. The black bands consist of acoustically focused 5 μm beads.

than for the other two. The presence of several local maxima is in agreement with the results of the 2D chamber model simulations. On the other hand, the strong coupling at 1.86 MHz could be interpreted as a support for the extended 1D model, where the local maxima could stem from the impedance of the mounted piezo's frequency dependence, or from the chip favoring coupling of certain frequencies. It is clear that more elaborate measurements are required in order to determine how well the different models agree with real devices.

C. Separation efficiency

The separation efficiency S was quantified at the three previously identified local acoustic maxima. S is defined as $S = P_{center}/P_{tot}$, where the number of particles collected from the center outlet P_{center} is divided by the total number of particles collected from all three outlets $P_{tot} = P_{center} + P_{waste}$. The transmitted power was set to 0.5 W for frequencies 1.96 MHz and 2.05 MHz, and to 0.2 W for 1.86 MHz. For each frequency, six samples were collected at three different flow rates. A more efficient separation was achieved for the frequency of 1.86 MHz than for the other two, see Fig. 4. However, by adjusting the acoustic power and the flow rate, it was possible (at least apparent to visual inspection) to achieve close to complete separation at all frequencies.
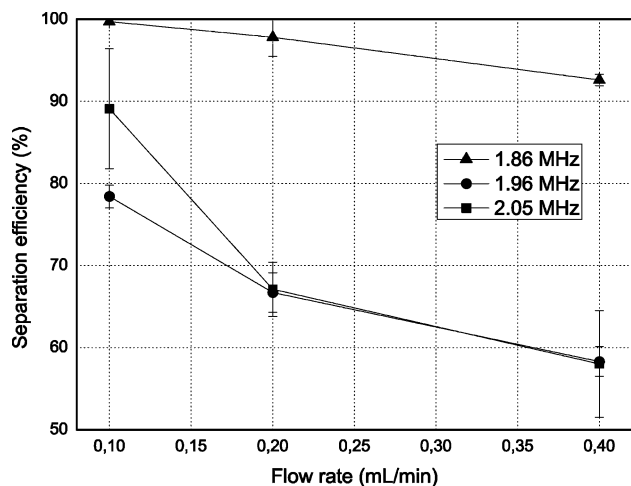
Fig. 4 Separation efficiency ($S = P_{center}/P_{tot}$) versus flow rate at three different frequencies.

The difference in separation efficiency between 1.96 MHz and 2.05 MHz at the flow rate of 0.1 mL min⁻¹ could be ascribed to a weaker total focusing effect along the separation channel for the lower frequency, even though it is not clearly visible in Fig. 3. Additionally, this deviation could also be explained by the presence of a local focusing asymmetry within the channel junction. For higher flow velocities, the particles are not sufficiently long within this part of the channel system to be notably affected by these forces. This assumption is in agreement with the micro-PIV measurements of the acoustic radiation force presented below (top of Fig. 5).
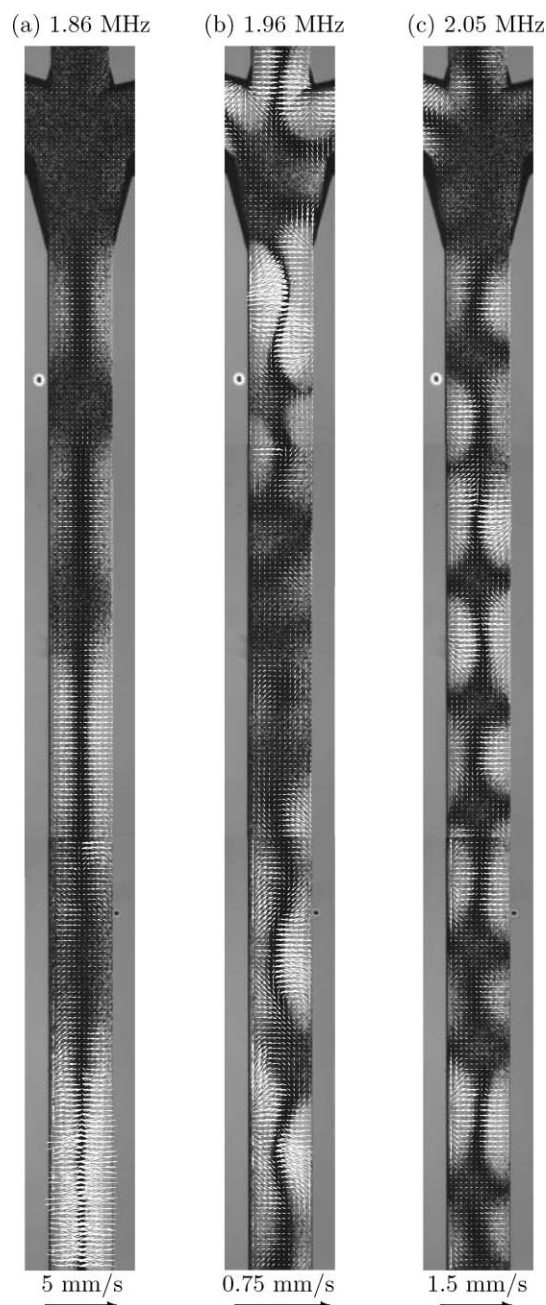
Fig. 5 Velocity vectors for particle displacements in zero flow caused by the acoustic radiation force superimposed on images of transient particle motion. (a) 1.86 MHz, 0.4 s, (b) 1.96 MHz, 2 s and (c) 2.05 MHz, 1 s. The number of pinching regions increases with the frequency. Reference vectors are shown at the bottom of each panel.

D. Measuring the acoustic radiation force with micro-PIV

When the microfluidic device is operated in flow-through mode, it is not possible to determine what the actual focusing patterns look like, since the continuous flow mode yields an image of the integrated acoustic effect along the full length of the separation channel. Therefore, in order to get a better understanding of the function of the device, more qualitative measurements are required. We apply the previously reported micro-PIV investigation approach,[16] where a combination of stop-flow and different sets of particles are used to distinguish and separate the acoustic effects. Furthermore, the identification of acoustic resonant patterns is facilitated if a larger section of the device can be examined. Of course, there is a tradeoff between low and high magnification, as a low magnification has its drawbacks in both reduced in-plane, and in-depth, resolution. Here, images were recorded at three partially overlapping positions, each with a total magnification of 3.15×, starting from the channel junction covering a distance approximately 6 mm upwards in the channel. In Fig. 5 the micro-PIV results of measurements performed with no external flow applied, but with the same frequencies and transmitted powers as were used in the flow-through measurements, are shown. The larger 5 µm particles were used, and thus, the velocity vectors are primarily showing motion of the particles caused by the acoustic radiation force.

Notably, the results are clearly favoring the 2D chamber model solutions compared to the extended 1D model. First of all, the velocity vectors are not all pointing directly towards the middle, and, thus, it is not solely a case of varying intensity along the length of the channel. Instead, the focusing is performed in certain pinching regions, as suggested by the chamber model. Secondly, the number of pinching regions is increasing with the frequency, which was also predicted by the chamber model (see Fig. 2).

From the measurements we can see that even though the 2D chamber model gives valuable and valid information about what the principal focusing pattern will look like, it is far from an exact representation of the actual resonant pattern formed in the system. This is because the acoustic resonances are not confined to the microfludic channels only, but are rather formed over the entire chip. An improved understanding of what the actual resonances may look like, can be given by a 2D chip model.[16] Two such solutions, solved for the measured dimensions of the whole device (Fig. 1), are shown in Fig. 6. These solutions are examples of global resonances that can explain the displacements and intensity irregularities of the patterns seen in the separation channel. However, it is important not to over-interpret the results of the chip model. In the actual situation there are several effects that are not taken into account by the model, such as irregular coupling from the resonator, discrepancies between the measured and actual dimensions of the device, overlapping of resonances, degenerations and 3D effects. In order to obtain a quantitative agreement, a full 3D simulation is required, including exact knowledge of the previously mentioned effects. Therefore, it is futile to search for an exact match between the measured displacements and the resonant patterns given by the 2D chip model. Nonetheless, the chip model has a value in the understanding of the formation of the acoustic resonances, although the principal solutions given by the simpler chamber
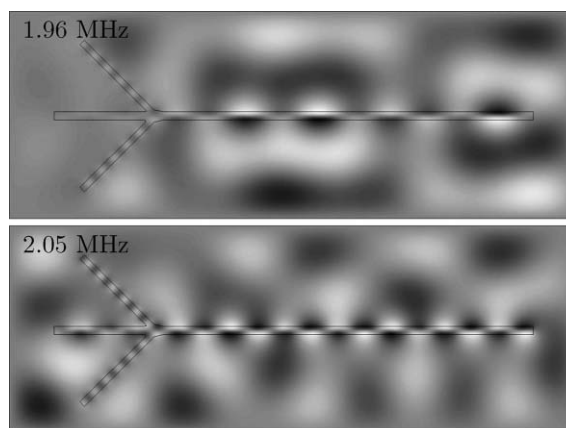
Fig. 6 Chip model simulations shown for two frequencies, supplying an illustration of what the pressure patterns forming over the whole chip may look like. In comparison with the chamber model, the patterns inside the channels are more irregular, which is in agreement with the experimental observations. Note that the model underestimates the number of pinching points in respect to the frequency in the measurements (and in the chamber model).

model can be of larger practical value in a process where a device is designed or characterized. In contrast, an extended 1D model has little practical value, and is often misleading.

E. Acoustic streaming results

So far, we have mainly focused on the acoustic radiation force, which is the acoustic effect utilized by the separation device. However, at the length scale of microfluidic devices, the acoustic radiation force is not the only acoustic effect which comes into play—acoustic streaming is also present.[20,21] Compared to the acoustic radiation force, which induces a movement of the particles relative to the medium, the acoustic streaming is a movement of the entire fluid. Since the acoustic radiation force scales with the volume of the particle, the streaming motion can generally be extracted by applying tracer particles of smaller size. In this study, we used 1 µm green fluorescent polystyrene spheres. Apart from the different particles, the streaming measurements were performed under similar conditions as for the micro-PIV measurements of the acoustic radiation force. The results are seen in Fig. 7.

As is evident, the streaming in the system is fairly weak compared to the much stronger acoustic radiation forces, and thus, it has minor influence on the functionality of this particular device. The streaming should, however, not be neglected, and for many micro-devices utilizing acoustic radiation forces, unwanted streaming could clearly pose a limitation to the function and efficiency of the same. For instance, streaming might be the limiting factor for the possibility to separate sub-micrometer particles. Also worth noticing is that there is no direct relation between the acoustic radiation force and the streaming, where in one part of the channel one can be strong whereas the other is not (comparing Fig. 5 and Fig. 7). All in all, it is our recommendation that micro-devices designed to utilize the acoustic radiation force also should be examined for the presence of streaming, especially in the case where the acoustic

(a) 1.86 MHz   (b) 1.96 MHz   (c) 2.05 MHz

50 μm/s
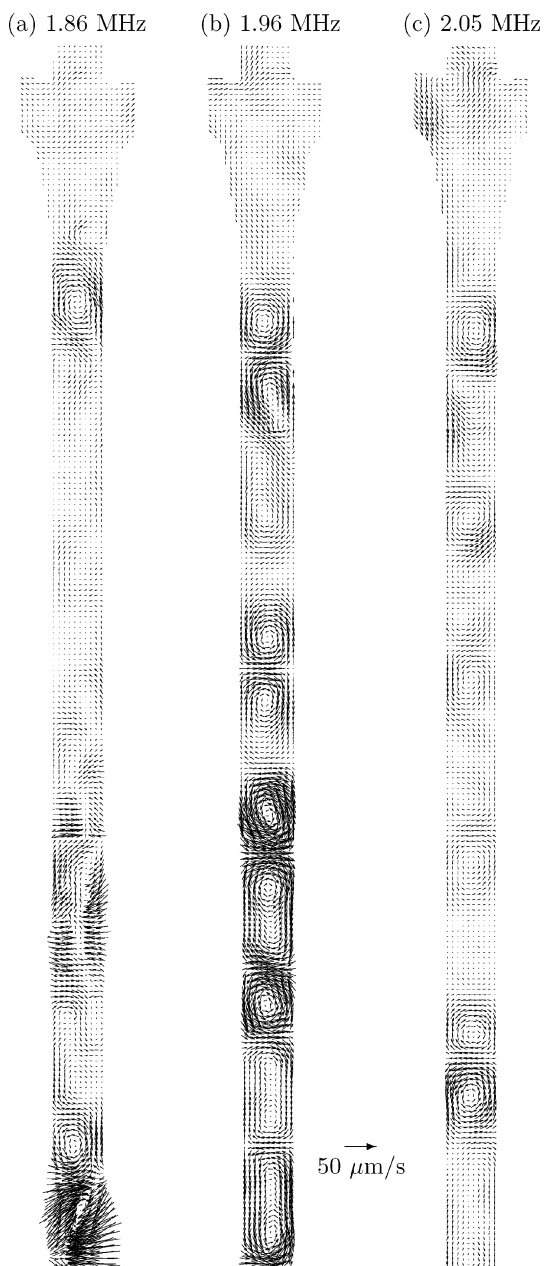
Fig. 7 Velocity vectors of fluid motion caused by acoustic streaming. 1 μm tracer particles were used for recordings at (a) 1.86 MHz, (b) 1.96 MHz and (c) 2.05 MHz. Reference vector is shown for 50 μm s^{-1}.

radiation force magnitude is low and particle translation also is governed by shearing effects, which commonly is the case for particle sizes of 1 μm or smaller.

IV.   Conclusion

The function of the chip investigated here is not critically depending upon the exactness of the applied forming acoustic resonances. When operated in flow-through mode, the more refined effects are not directly apparent, which is most likely the reason why they have been overlooked, and not investigated, in previous studies. However, for several proposed micro-devices utilizing acoustic forces (especially for higher order of functionality such as successive separation stages and handling of live cells) the local effects are of great importance to the outcome, and, thus, the overall success of the device. If the local effects are not understood and controlled, these devices have little chance of making it beyond the proof of principle stage in the research lab. Therefore, we suggest that the extended 1D visualizations of acoustic coupling in microfluidic devices should be avoided, since they provide a misleading description of the phenomena in these devices.

Instead, at least a simple 2D model should be considered and included. The reported 2D model provides improved means to understand the acoustic resonance effects obtained in microfluidic acoustic resonators. Yet, further modeling improvements are needed in order to supply an efficient design tool. Furthermore, our results have shown the importance of performing qualitative spatial measurements (such as those provided by the micro-PIV method) of the forming acoustic patterns, since the actual outcome of the acoustic actuation is difficult to predict. This is especially important for devices where the effect is intended to be confined to a much smaller spatial region than what is the case in the acoustic separator device examined here.

References

1 K. Yasuda, S. Umemura and K. Takeda, *Jpn. J. Appl. Phys., Part 1*, 1995, **34**, 2715.
2 K. Yasuda, K. Takeda and S. Umemura, *Jpn. J. Appl. Phys., Part 1*, 1996, **35**, 3295.
3 X. Zhu and E. S. Kim, *Sens. Actuators, A*, 1998, **66**, 355.
4 Z. Yang, S. Matsumoto, H. Goto, M. Matsumoto and R. Maeda, *Sens. Actuators, A*, 2001, **93**, 266.
5 M. Saito, N. Kitamura and M. Terauchi, *J. Appl. Phys.*, 2002, **92**, 7581.
6 T. Lilliehorn, U. Simu, M. Nilsson, M. Almqvist, T. Stepinski, T. Laurell, J. Nilsson and S. Johansson, *Ultrasonics*, 2005, **43**, 293.
7 F. Petersson, A. Nilsson, H. Jonsson and T. Laurell, *Anal. Chem.*, 2005, **77**, 1216.
8 A. Nilsson, F. Petersson, H. Jonsson and T. Laurell, *Lab Chip*, 2004, **4**, 131.
9 H. Jonsson, C. Holm, A. Nilsson, F. Petersson, P. Johns-son and T. Laurell, *Ann. Thorac. Surg.*, 2004, **78**, 1572.
10 H. Li and T. Kenny, *Conf. Proc. 26 Ann. Int. Conf. IEEE. Engineering, in Medicne and Biology*, 2004, **3**, 2631, vol. 4.
11 J. J. Hawkes, R. W. Barber, D. R. Emerson and W. T. Coakley, *Lab Chip*, 2004, **4**, 446.
12 F. Petersson, L. Aberg, A.-M. Sward-Nilsson and T. Laurell, *Anal. Chem.*, 2007, **79**, 5117.
13 L. V. King, *Proc. R. Soc. London, Ser. A*, 1934, **147**, 212.
14 K. Yosioka and Y. Kawasima, *Acustica*, 1955, **5**, 167.
15 L. P. Gorkov, *Sov. Phys. Dokl.*, 1962, **6**, 773.
16 S. M. Hagsäter, T. Glasdam Jensen, H. Bruus and J. P. Kutter, *Lab Chip*, 2007, **7**, 1336.
17 F. Petersson, A. Nilsson, C. Holm, H. Jonsson and T. Laurell, *Analyst*, 2004, **129**, 938.
18 T. Laurell, F. Petersson and A. Nilsson, *Chem. Soc. Rev.*, 2007, **36**, 492.

19 S. M. Hagsäter, C. H. Westergaard, H. Bruus and J. P. Kutter, *Exp. Fluids*, 2008, **44**, 211.
20 Lord Rayleigh, *Proc. R. Soc. London*, 1883, **36**, 10.
21 N. Riley, *Annu. Rev. Fluid Mech.*, 2001, **33**, 43.
22 J. F. Spengler, M. Jekel, K. T. Christensen, R. J. Adrian, J. J. Hawkes and W. T. Coakley, *Bioseparation*, 2001, **9**, 329.
23 J. F. Spengler, W. T. Coakley and K. T. Christensen, *AIChE J.*, 2003, **49**, 2773.
24 L. A. Kuznetsova and W. T. Coakley, *J. Acoust. Soc. Am.*, 2004, **116**, 1956.
25 L. A. Kuznetsova, S. Khanna, N. N. Amso and W. T. Coakley, *J. Acoust. Soc. Am.*, 2005, **117**, 104.